minerals

MDPI

Article

Geochronology and Geochemistry of the Wulanwuzhuer Intermediate–Felsic Intrusion from Qimantag Area, East Kunlun Mountains: Implications for Regional Tectonic Evolution

Maoguo An [1,2,3,4], Junjin Zhang [4], Qinglin Xu [5,*], Yanqian Yang [6,7], Ziyi Dong [5] and Guangzhou Mao [5]

1 School of Earth Sciences and Resources, China University of Geosciences, Beijing 100083, China; 287318621@163.com
2 State Key Laboratory of Geological Processes and Mineral Resources, China University of Geosciences, Beijing 100083, China
3 Frontiers Science Center for Deep-Time Digital Earth, China University of Geosciences, Beijing 100083, China
4 Shandong Provincial No. 3 Exploration Institute of Geology and Mineral Resources, Yantai 264004, China; zhjj109@163.com
5 College of Earth Science and Engineering, Shandong University of Science and Technology, Qingdao 266590, China; 15064302100@163.com (Z.D.); gzmaonjunwu@163.com (G.M.)
6 Qinghai Geological Survey, Xining 810001, China; qhddjyyq@163.com
7 Technology Imnouation Center for Exploration and Exploitation of Strategic Mineral Resources in Plateau Desert Region, Ministry of Natural Resources, Xining 810001, China
* Correspondence: xql_618@163.com

Abstract

A vast suite of intermediate–felsic intrusive rocks, the Wulanwuzhuer intrusion, which intrude the Jinshuikou Group in the Qimantag area of the Eastern Kunlun Mountains, Qinghai Province, has an unclear formation age and petrogenesis. In this paper, we discuss their formation time, petrogenesis, and tectonic background. Based on detailed field geological surveys, this paper presents zircon U-Pb isotope chronology and petrogeochemistry to identify the genesis of rocks, determine the intrusion age, and explore their tectonic significance. The Wulanwuzhuer rocks are composed of fine-grained granodiorite, gneissic biotite granite and potassic granite. Zircon LA-ICP-MS U-Pb dating of zircon yields an age of 475 ± 2 Ma for the gneissic biotite granite. This indicates a Caledonian formation age, contrasting with the previously assumed Hercynian age. The Wulanwuzhuer rocks show SiO_2 contents that vary from 62% to 74%, K_2O varies from 4.0% to 5.2%, K_2O/Na_2O varies from 1.41 to 6.29, and A/CNK varies from 0.79 to 1.26. The rocks are weakly peraluminous to metaluminous and belong to the shoshonitic series. These geochemical signatures suggest that the formation of the Wulanwuzhuer rocks was predominantly influenced by subduction-related processes, including metasomatism by fluids derived from the subducted oceanic slab. Contributions from an enriched mantle source, as indicated by LILE and LREE enrichment, also played a role. Combined with the age and tectonic evolution, it is concluded that these rocks were formed at an island arc-type active continental margin, which is a response of the Proto-Tethys oceanic crust subducting beneath the Qaidam massif from south to north along the vicinity of modern Kunzhong Fault in the Early Caledonian.

Keywords: Wulanwuzhuer intermediate–acidic intrusive rocks; geochemistry; Zircon LA-ICP-MS U-Pb ages; Qimantag area; Eastern Kunlun Mountains

Check for updates

Received: 30 December 2025
Revised: 27 February 2026
Accepted: 27 February 2026
Published: 2 March 2026

Copyright: © 2026 by the authors. Licensee MDPI, Basel, Switzerland. This article is an open access article distributed under the terms and conditions of the Creative Commons Attribution (CC BY) license.

1. Introduction

The East Kunlun Orogenic Belt (EKOB), situated on the southern margin of the Qaidam Block [1,2], forms the western segment of the Central Orogenic Belt of China [3–5]. It is commonly subdivided by three approximately E–W-trending, parallel major fault zones into three tectonic units: the North East Kunlun, Central East Kunlun, and South East Kunlun belts [3,6]. Sun et al. (2003) [7] interpreted the geological significance of these three tectonic belts as the North East Kunlun Caledonian back-arc rift zone, the Central East Kunlun basement uplift and granite zone, and the South East Kunlun composite accretionary zone, respectively. This orogen has experienced multiple episodes of orogeny, resulting in a complex geodynamic evolution history [3,5,8–13].

The Qimantag area, which is the subject of the study, is located in the western segment of the East Kunlun Orogenic Belt and constitutes an important part of the East Kunlun Metallogenic Belt. In recent years, the discovery of several deposits closely associated with intermediate–felsic intrusive rocks in this area (e.g., the Baiganhu tungsten–tin deposit, the Wulanwuzhuer copper deposit, the Kaerqueka Yelasa copper deposit, and the Suolajier copper polymetallic deposit) has attracted significant scholarly attention [14,15]. The Wulanwuzhuer area, situated in the eastern part of Qimantag, was the site of intense magmatic activity and is a key region for polymetallic hydrothermal copper–tin mineralization, making it a critical area for studying the magmatic and metallogenic processes within the East Kunlun Orogenic Belt [14]. However, previous research on magmatism in this region has predominantly focused on the Hercynian–Indosinian period [5,10,16–26], while studies on Caledonian magmatic activity are relatively limited and have mainly addressed the late Caledonian epoch [27–33]. This study presents geochronological and geochemical data for the intermediate–felsic intrusive rocks in the Wulanwuzhuer area, with the aim of investigating their petrogenesis and the tectonic setting of their formation, thereby seeking to enhance the understanding of early Caledonian tectono-magmatic activity in this region.

2. Geological Setting and Sample Characteristics

The EKOB lies on the western segment of the Central Orogenic Belt and is bounded by the Qaidam Block to the north and the Bayan Har-Songpanganzi Terrane to the south (Figure 1a,b). The EKOB trends E–W and extends for 1500 km with a width of 50–200 km. The EKOB is divided into the following three main units: the North Kunlun Belt (NKB), the Central Kunlun Belt (CKB), and the South Kunlun Belt (SKB) (Figure 1). The boundaries between the three units are the North, Center, and South Kunlun Faults [7]. The Wulanwuzhuer area is situated within the North Kunlun Caledonian Back-Arc Rift Zone, a secondary tectonic unit of the East Kunlun Orogenic Belt (Figure 2). The exposed strata in the Wulanwuzhuer area include medium- to high-grade metamorphic rocks of the Baishahe Formation of the Paleoproterozoic Jinshuikou Group, and marine shallow-metamorphic rocks of the Langyashan Formation, which together constitute the crystalline basement of the region. Overlying these are Paleozoic sequences of the Qimantag Group (Tanjianshan Group), which comprise andesite, greenschist, and tuff intercalated with phyllite and marble. Early Mesozoic strata are widely represented by Late Triassic continental intermediate–felsic pyroclastic rocks, with basal sequences consisting of intermediate–mafic volcanic rocks, acidic volcanic rocks, and intercalated clastic rocks.

The fault structures in the area are well developed. Regional-scale faults predominantly trend NW and are mainly thrust faults, supplemented by NE- and NNE-trending faults. The NW-trending faults, together with secondary NW-, NNW-, and NEE-trending faults, form a network-like fault system. Magmatic activity in the region was intense and characterized by multiple episodes. Intrusive rocks include mid-Caledonian gabbro and late-Caledonian granite, as well as Hercynian and Indosinian–Yanshanian porphyritic

biotite monzogranite, porphyritic monzogranite, and quartz-biotite diorite. The Wulanwuzhuer intermediate–felsic intrusion is located primarily to the southwest of the Wulanwuzhuer copper deposit, occurring as a large composite pluton. The main rock types consist of medium- to fine-grained Monzonitic granite, gneissic biotite granite and potassic granite (Figure 2). Previous studies reported a crystallization age of 421.2 ± 1.9 Ma (MSWD = 2.1, n = 32) for the potassic granite [14].

The samples selected for this work are gneissic biotite granite. The gneissic biotite granite has a light reddish-gray fresh surface, with a granitic texture and gneissic structure. The granite is composed of quartz (~30%), alkali feldspar (~35%), plagioclase (~20%), and biotite (~10%); accessory minerals account for about 5%, mainly sphene, apatite, and zircon. Feldspar and quartz are relatively evenly distributed as granular crystals, while biotite is oriented between the felsic minerals, giving the rock its gneissic structure. The granodiorite has a grayish-white fresh surface, with a medium- to fine-grained texture and massive structure. Its main mineral composition includes quartz (20%–25%), alkali feldspar (15%–20%), plagioclase (30%–40%), amphibole (~10%), and biotite (~3%); accessory minerals are zircon, sphene, and minor opaque minerals.

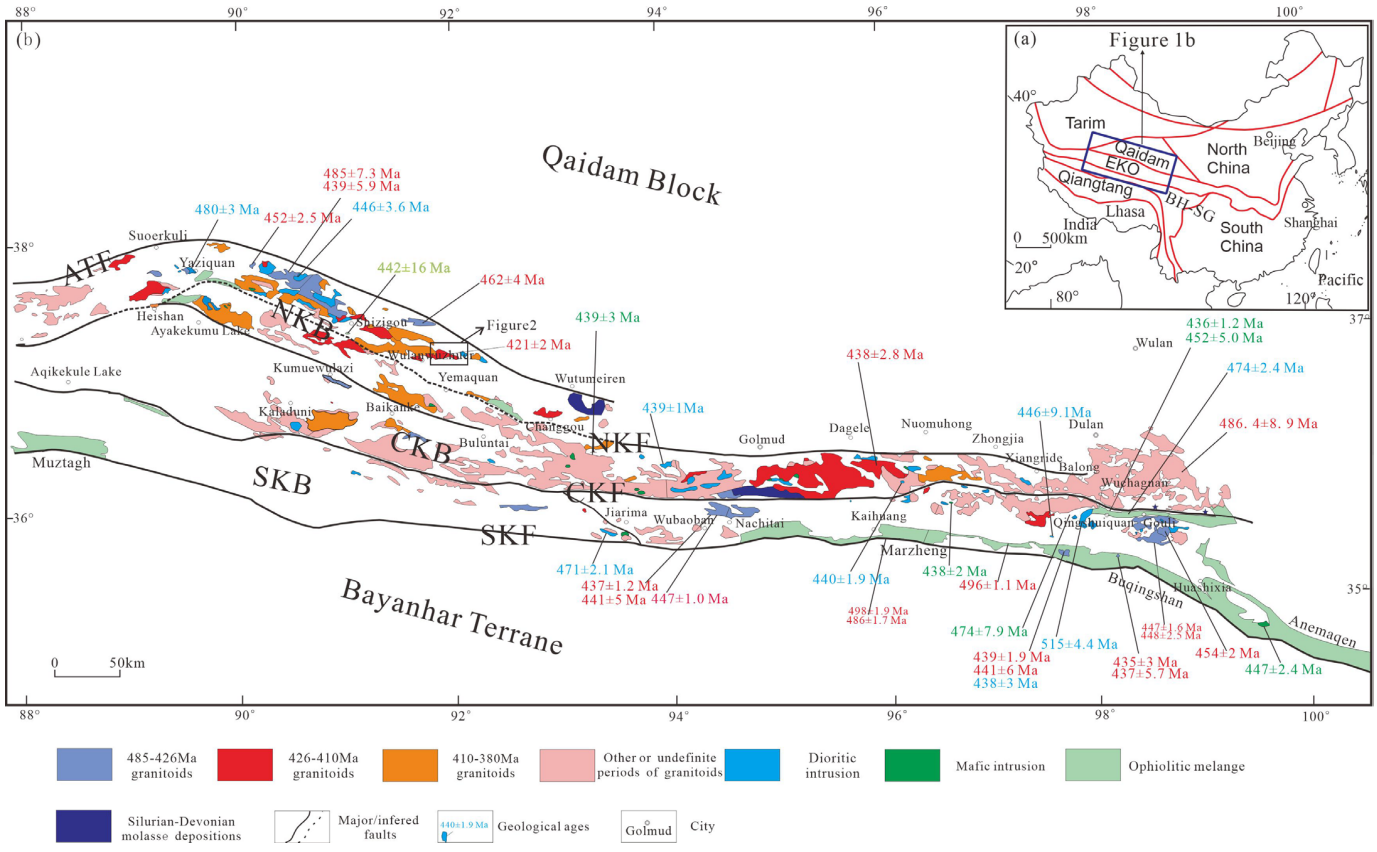

Figure 1. (**a**) Tectonic map of China (after [34]); (**b**) schematic geological map of the Eastern Kunlun Orogen Belt (after [35]). The ages of the intrusions shown in the figure are taken from Supplementary Table S1, and the colors of the ages are consistent with the colors of the intrusions on the geological map.

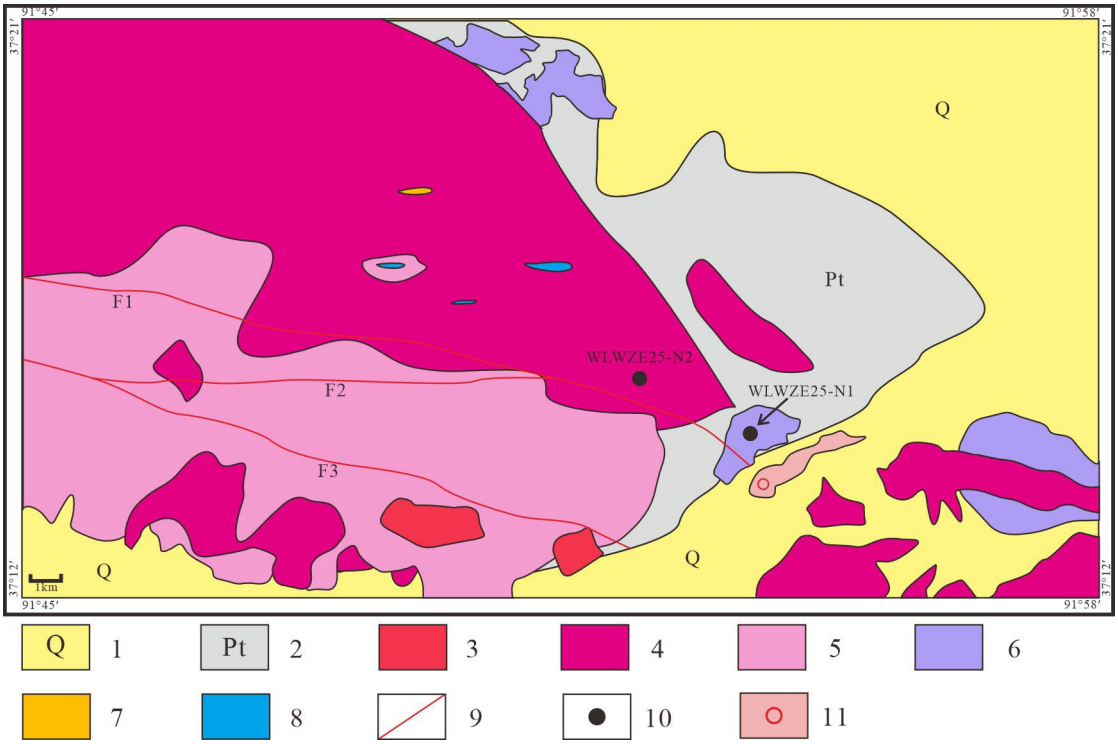

Figure 2. Geology of the study area (after [36]). Legend: 1. Quaternary system; 2. gneiss of the Jinshuikou group; 3. biotite K-feldspar granite; 4. medium-fine-grained monzonitic granite; 5. porphyritic medium–fine-grained monzonitic granite; 6. gneissic biotite granite; 7. diorite dike; 8. diabase dike; 9. fault; 10. sampling location; 11. potassium granite and the sample location of Hao et al., 2015 [14]. F1, F2 and F3 are three fractures.

3. Analytical Methods

3.1. Zircon U-Pb Geochronology

Zircon separation was conducted at the Laboratory of the Langfang Regional Geological Survey Institute, Hebei Province. The separated zircon grains were handpicked under a binocular microscope to select those with flat, clean surfaces, varying length-to-width ratios, distinct prism and pyramid faces, and different colors. The selected grains were mounted in colorless, transparent epoxy resin. After the resin hardened, the mount was polished to expose the cores of the zircon grains. Cathodoluminescence (CL) imaging and LA-ICP-MS U-Pb dating of the zircon grains were performed at the State Key Laboratory of Continental Dynamics, Northwest University. Prior to in situ analysis, the crystal morphology and internal structures of the zircons were examined in detail using reflected light and CL images to identify the optimal locations for isotope analysis. The U-Pb dating was carried out using an Agilent 7500a ICP-MS coupled with a GeoLas-193 ultraviolet laser ablation system. The analysis employed a single-spot ablation mode, with helium as the carrier gas. The laser spot size was 30 μm, operating at a frequency of 8 Hz. Data acquisition for ICP-MS utilized a peak-hopping mode. The standard zircon 91,500 and the reference material NIST 610 were analyzed after every six sample spots. The isotopic ratio data were processed for mass bias correction using the standard zircon 91,500 as an external standard. Raw data reduction was performed using the GLITTER (ver. 4.0) program. The corrected data were then processed for common lead correction using the ICPMSDataCal 7.7 [37]. The final U-Pb ages were calculated and concordia diagrams were generated using the Isoplot program [38]. Element concentrations were calibrated using NIST 610 as the

external standard and Si as the internal standard. Detailed procedures for LA-ICP-MS analysis and data processing followed those described in the references [39,40].

3.2. Whole-Rock Geochemistry

Whole-rock major, trace and REE analyses were conducted at the Center of Test Science, Jilin University. Major element concentrations were determined using X-ray fluorescence spectrometry (XRF, model PW1404/10) following Chinese national standard GB/T 14506.28-93 [41], with relative standard deviations (RSDs) between 2% and 5%. Trace element and rare earth element (REE) concentrations were analyzed using an Agilent 7500A inductively coupled plasma–mass spectrometer (ICP-MS; Agilent Technologies, Santa Clara, CA, USA) following standard guideline DZ/T0223-2001 [42]. Analytical accuracy was monitored using international reference materials BHVO-2 and BCR-2, along with Chinese national reference materials GBW07103 [43] and GBW07104 [44]. The analytical precision was as follows: for elements with concentrations greater than 10×10^{-6}, the relative error was less than 5%; for elements with concentrations less than 10×10^{-6}, the relative error was less than 10%.

4. Results

4.1. Zircon U-Pb Geochronology

The sample for zircon dating was the gneissic biotite granite. Zircon grains from the sample are generally large (100–150 μm in length), with a high degree of euhedral crystal formed. They predominantly occur as prisms terminated by bipyramids, forming combinations of tetragonal prisms and dipyramids or complex tetragonal dipyramids; a few grains are anhedral or fragmented. The length-to-width ratios typically range from 2:1 to 5:1. In cathodoluminescence (CL) images (Figure 3), the zircon crystals exhibit homogeneous internal structures and well-developed oscillatory zoning. They show a wide range of Th (361–1565 ppm) and U (1115–4620 ppm) contents (Table 1), with Th/U ratios ranging from 0.2 to 0.4, and show typical characteristics of magmatic zircon with Th/U > 0.1.

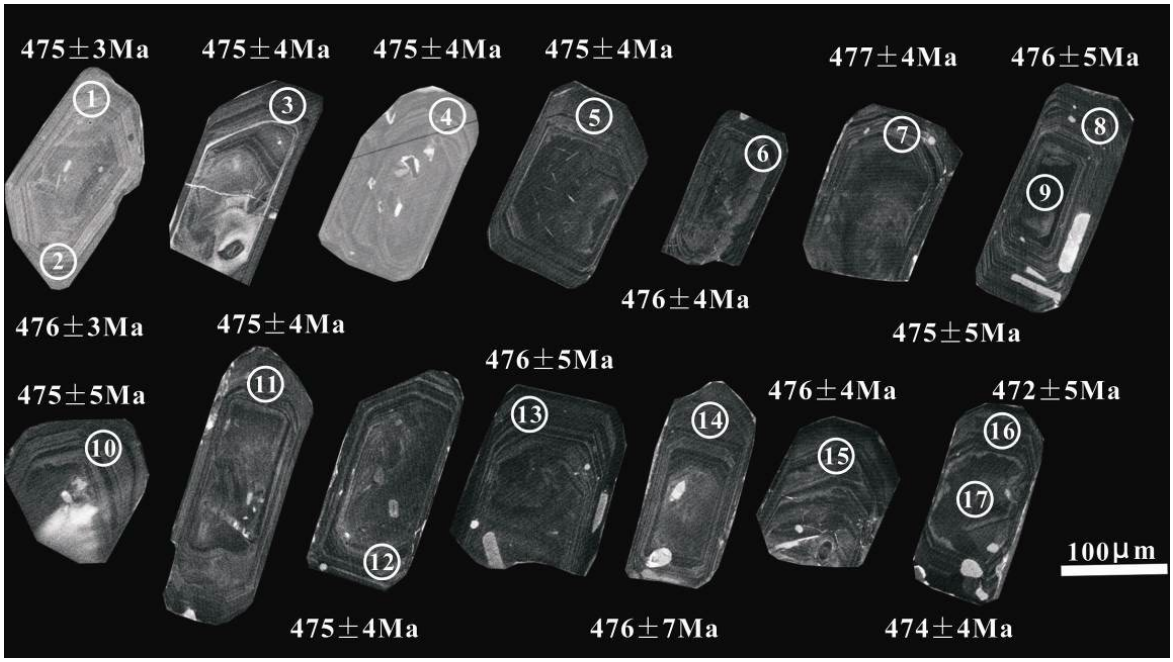

Figure 3. CL images of zircons from Wulanwuzhuer gneissic biotite granite. The numbers in the figure represent the laser ablation spots.

Table 1. Zircon U-Pb dating of gneissic granite from the Wulanwuzhuer region.

Analysis	Pb	Th	U	$^{232}Th/^{238}U$	$^{207}Pb/^{206}Pb$		$^{207}Pb/^{235}U$		$^{206}Pb/^{238}U$		$^{207}Pb/^{206}Pb$		$^{207}Pb/^{235}U$		$^{206}Pb/^{238}U$		$^{208}Pb/^{232}Th$	
	ppm	ppm	ppm		Ratio	1σ	Ratio	1σ	Ratio	1σ	Age (Ma)	1σ	Age (Ma)	1σ	Age (Ma)	1σ	Age (Ma)	1σ
WLWZE25-N1-01	221.0	933.8	2575.2	0.36	0.05520	0.00075	0.58377	0.00847	0.07655	0.00045	420	30	467	5	475	3	470	7
WLWZE25-N1-02	209.8	830.8	2443.5	0.34	0.05699	0.00077	0.60317	0.00905	0.07662	0.00056	491	30	479	6	476	3	484	8
WLWZE25-N1-03	317.9	1246.1	3641.9	0.34	0.05790	0.00090	0.61215	0.01040	0.07654	0.00066	526	33	485	7	475	4	500	10
WLWZE25-N1-04	240.1	800.5	2825.4	0.28	0.05604	0.00080	0.59177	0.00896	0.07647	0.00059	454	30	472	6	475	4	490	9
WLWZE25-N1-05	302.3	760.9	3720.6	0.20	0.05667	0.00078	0.59839	0.00866	0.07651	0.00066	479	26	476	5	475	4	496	10
WLWZE25-N1-06	325.2	1287.7	3887.8	0.33	0.05441	0.00075	0.57664	0.00848	0.07666	0.00059	388	29	462	5	476	4	464	8
WLWZE25-N1-07	234.8	1055.6	2764.2	0.38	0.05430	0.00082	0.57646	0.00930	0.07673	0.00060	383	32	462	6	477	4	464	8
WLWZE25-N1-08	259.7	1040.1	3140.0	0.33	0.05551	0.00085	0.58812	0.00994	0.07665	0.00077	433	31	470	6	476	5	475	10
WLWZE25-N1-09	180.6	832.6	2201.7	0.38	0.05531	0.00093	0.58437	0.01061	0.07647	0.00076	425	35	467	7	475	5	472	10
WLWZE25-N1-10	212.8	934.4	2523.0	0.37	0.05706	0.00087	0.60249	0.01024	0.07650	0.00084	494	29	479	6	475	5	491	9
WLWZE25-N1-11	331.3	1564.6	3867.6	0.40	0.05788	0.00079	0.61145	0.00871	0.07650	0.00059	525	27	484	5	475	4	486	7
WLWZE25-N1-12	303.0	1345.5	3601.0	0.37	0.05678	0.00080	0.59834	0.00896	0.07639	0.00062	483	28	476	6	475	4	477	7
WLWZE25-N1-13	339.9	1295.3	4116.8	0.31	0.05535	0.00087	0.58458	0.01013	0.07657	0.00077	426	32	467	6	476	5	464	8
WLWZE25-N1-14	92.2	361.4	1115.4	0.32	0.05860	0.00166	0.61003	0.01214	0.07663	0.00111	552	30	484	8	476	7	528	27
WLWZE25-N1-15	246.8	790.4	3021.6	0.26	0.05644	0.00078	0.59776	0.00920	0.07663	0.00069	470	28	476	6	476	4	476	8
WLWZE25-N1-16	385.3	1148.1	4619.9	0.25	0.05736	0.00177	0.60129	0.01734	0.07603	0.00082	505	69	478	11	472	5	472	5
WLWZE25-N1-17	245.7	947.3	2890.7	0.33	0.05676	0.00126	0.59698	0.01242	0.07628	0.00059	482	50	475	8	474	4	474	4

Fourteen representative grains displaying clear oscillatory zoning were selected for U-Pb dating, resulting in 17 analytical spots. The analytical data points fall on or near the concordia curve (Figure 4), except for samples N1-6 and N1-7, which were excluded from the age calculation, indicating an absence of significant Pb loss and confirming the magmatic origin of the zircons [40]. The 15 spot analyses yield a weighted mean $^{206}Pb/^{238}U$ age of 475.1 ± 2.1 Ma (MSWD = 0.049) and a concordia age of 475.2 ± 1.0 Ma (MSWD = 0.03). These two ages are consistent within error and are interpreted to represent the crystallization age of the intrusion, corresponding to the Middle Ordovician.

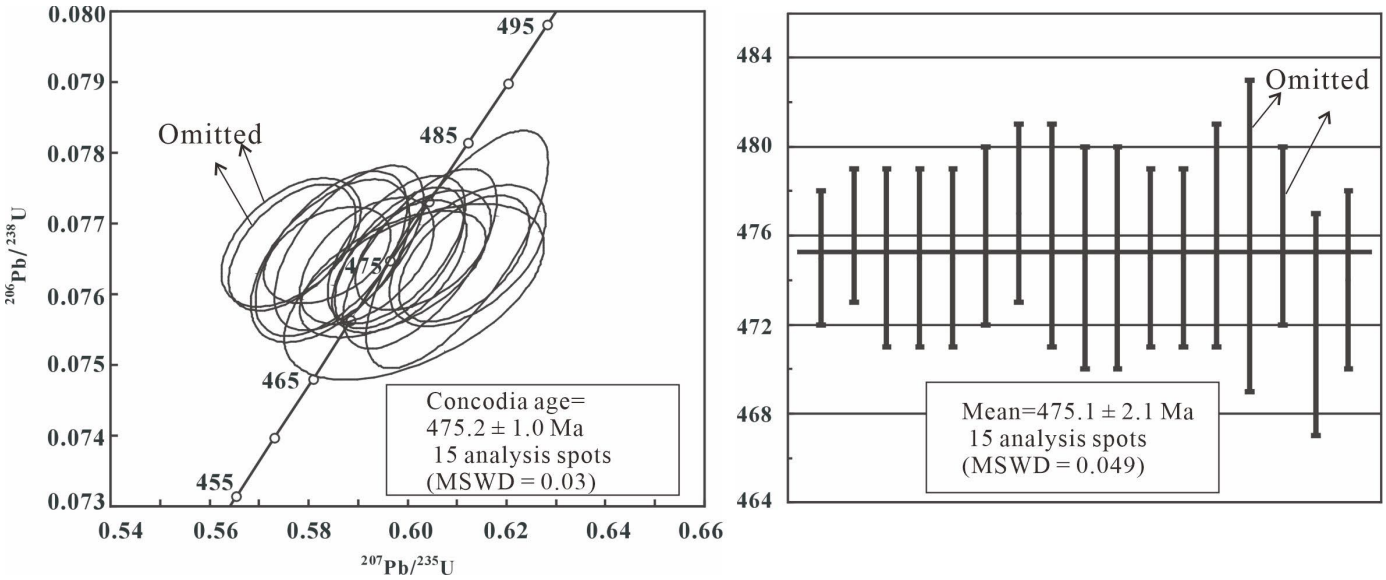

Figure 4. Concordia diagram of U-Pb data for zircons of Wulanwuzhuer gneissic biotite granite.

4.2. Whole-Rock Geochemistry

The results of major and trace element analyses are presented in Table 2. The rocks have SiO_2 contents ranging from 62.18% to 74.29%, classifying them as intermediate–felsic to felsic in composition. They are characterized by high potassium (K_2O = 4.00%–5.20%, avg. 4.74%) and low sodium (Na_2O = 0.73%–2.84%, avg. 1.76%) contents, with K_2O/Na_2O ratios between 1.41 and 6.29. The total alkali contents are relatively high [($Na_2O + K_2O$) = 5.32%–7.22%]. The rocks are also aluminous (Al_2O_3 = 11.78%–14.38%, avg. 13.07%). They exhibit low concentrations of MgO (0.67%–3.96%, avg. 2.3%; $Mg^{\#}$ = 33–50), CaO (1.74%–3.89%, avg. 2.87%), and TiO_2 (0.35%–1.15%, avg. 0.74%). On the TAS diagram, the samples plot in the granite and granodiorite fields (Figure 5a). On the AFM diagram, all samples fall within the calc-alkaline series field (Figure 5b). The A/CNK versus A/NK diagram (Figure 5c) indicates that the rocks are predominantly weakly peraluminous to metaluminous, with A/CNK values ranging mainly from 0.79 to 1.26. On the SiO_2 versus K_2O diagram (Figure 5d), granodiorites plot in the field of the shoshonitic series whereas the gneissic granites plot in the field of the calc-alkaline series.

Table 2. Major (wt %) and trace ($\times 10^{-6}$) element compositions of the intermediate–acidic intrusive rocks from Wulanwuzhuer area.

Sample No.	WLWZE25-N1-1	WLWZE25-N1-2	WLWZE25-N1-3	WLWZE25-N2-1	WLWZE25-N2-2	WLWZE25-N2-3	WLWZE25-N2-4	WLWZE25-N2-5	WLWZE25-N2-6	Detection Limit
SiO_2	72.30	70.75	74.29	62.49	62.18	63.28	61.44	63.88	63.44	
TiO_2	0.35	0.48	0.35	0.81	0.74	0.78	1.15	1.00	1.04	
Al_2O_3	13.28	13.17	12.18	14.38	14.21	14.31	11.78	12.20	12.10	
Fe_2O_3	0.17	0.57	0.25	1.76	1.70	2.37	2.32	1.49	1.48	
FeO	2.32	2.53	2.03	5.27	6.30	5.68	5.81	5.07	5.32	
MnO	0.08	0.09	0.06	0.18	0.18	0.19	0.21	0.18	0.17	
MgO	0.68	0.86	0.67	2.46	2.34	2.45	3.96	3.61	3.66	
CaO	1.79	2.18	1.74	3.60	2.38	2.85	3.71	3.89	3.66	
Na_2O	2.16	1.83	2.18	0.91	2.84	0.73	1.56	1.79	1.88	
K_2O	5.06	4.71	4.38	4.94	4.00	4.59	5.20	4.78	5.03	
P_2O_5	0.15	0.20	0.16	0.35	0.33	0.35	0.46	0.38	0.41	
LOI	1.09	2.45	1.05	1.87	1.94	1.61	2.04	1.43	1.58	
Total	99.43	99.82	99.34	99.02	99.14	99.19	99.64	99.7	99.77	
$Mg^{\#}$	33	34	35	39	35	36	47	50	50	
$K_2O + N_2O$	7.22	6.54	6.56	5.85	6.84	5.32	6.76	6.57	6.91	
K_2O/N_2O	2.34	2.57	2.01	5.43	1.41	6.29	3.33	2.67	2.68	
A/CNK	1.08	1.09	1.06	1.07	1.07	1.26	0.79	0.80	0.80	
Sc	5.40	6.42	5.66	18.8	16.6	17.6	25.9	24.6	21.9	0.04672
V	29.8	39.3	29.7	117	109	109	149	139	126	0.01462
Cr	9.00	12.4	7.60	59.8	51.7	56.7	11.7	10.3	9.90	0.12202
Co	4.75	5.43	4.26	16.8	18.4	24.6	23.9	21.5	19.8	0.007616
Ni	7.15	6.68	6.68	15.8	15.5	15.5	3.40	3.30	2.80	0.10552
Zn	466	114	260	193	228	441	79.5	58.1	59.4	0.06516
Rb	289	304	266	376	399	361	311	296	304	0.005554
Sr	108	107	105	284	235	223	233	310	253	0.02136
Zr	171	260	220	279	249	269	421	303	402	0.07272
Nb	20.9	25.1	21.7	27.3	29.7	27.9	43.0	36.1	34.9	0.00703
Ba	496	507	424	1140	672	960	996	876	745	0.0595
Ta	3.19	3.21	3.58	1.82	3.61	2.36	1.87	1.48	1.69	0.0014776
Pb	85.1	51.7	66.0	46.0	26.3	28.9	34.7	23.7	25.4	0.009766
Th	39.4	39.4	43.8	27.6	24.4	33.1	59.1	39.9	45.1	0.012916
U	15.2	13.3	15.2	2.20	2.33	3.79	11.1	20.3	4.90	0.014556
Y	33.4	42.6	39.1	32.0	41.7	36.4	49.3	40.8	43.2	0.009632
La	70.2	75.9	80.1	74.5	86.2	108	120	90.6	97.6	0.0008554
Ce	142	148	162	142	162	203	234	175	189	0.010662
Pr	16.1	17.1	18.6	15.6	18.2	22.4	25.4	19.1	20.3	0.010398
Nd	56.4	59.2	64.0	57.0	66.3	78.3	92.7	70.3	73.4	0.016572
Sm	10.1	10.2	11.7	10.1	11.6	12.8	15.4	11.5	12.1	0.0305
Eu	0.86	1.04	0.85	1.83	1.96	2.00	1.89	1.57	1.47	0.008552
Gd	7.62	8.41	8.65	7.78	9.24	9.48	12.9	10.2	10.4	0.012242
Tb	1.20	1.44	1.39	1.18	1.46	1.50	1.80	1.44	1.46	0.0007878
Dy	6.78	8.68	7.75	6.68	8.54	7.99	10.0	8.10	8.40	0.011986
Ho	1.27	1.65	1.42	1.22	1.58	1.50	1.86	1.48	1.55	0.005814
Er	3.28	4.61	3.81	3.25	4.21	3.78	5.29	4.31	4.59	0.006834
Tm	0.52	0.75	0.64	0.50	0.66	0.55	0.79	0.62	0.66	0.006254
Yb	3.05	4.40	3.82	2.89	3.70	3.18	4.89	3.96	4.39	0.17088
Lu	0.46	0.64	0.59	0.44	0.53	0.46	0.75	0.60	0.67	0.00547
ΣREE	319	342	365	325	376	456	528	399	426	
LREE	295	312	337	301	346	427	490	368	394	
HREE	24.2	30.6	28.1	23.9	29.9	28.4	38.3	30.8	32.1	
LREE/HREE	12.2	10.2	12.0	12.6	11.6	15.0	12.8	12.0	12.3	
Rb/Sr	2.68	2.84	2.53	1.32	1.70	1.62	1.33	0.95	1.20	
Nb/Ta	6.55	7.82	6.06	15.0	8.23	11.8	23.0	24.4	20.7	
$(La/Yb)_N$	16.5	12.4	15.1	18.5	16.7	24.4	17.7	16.4	16.0	
δEu	0.29	0.33	0.25	0.61	0.56	0.53	0.40	0.43	0.39	

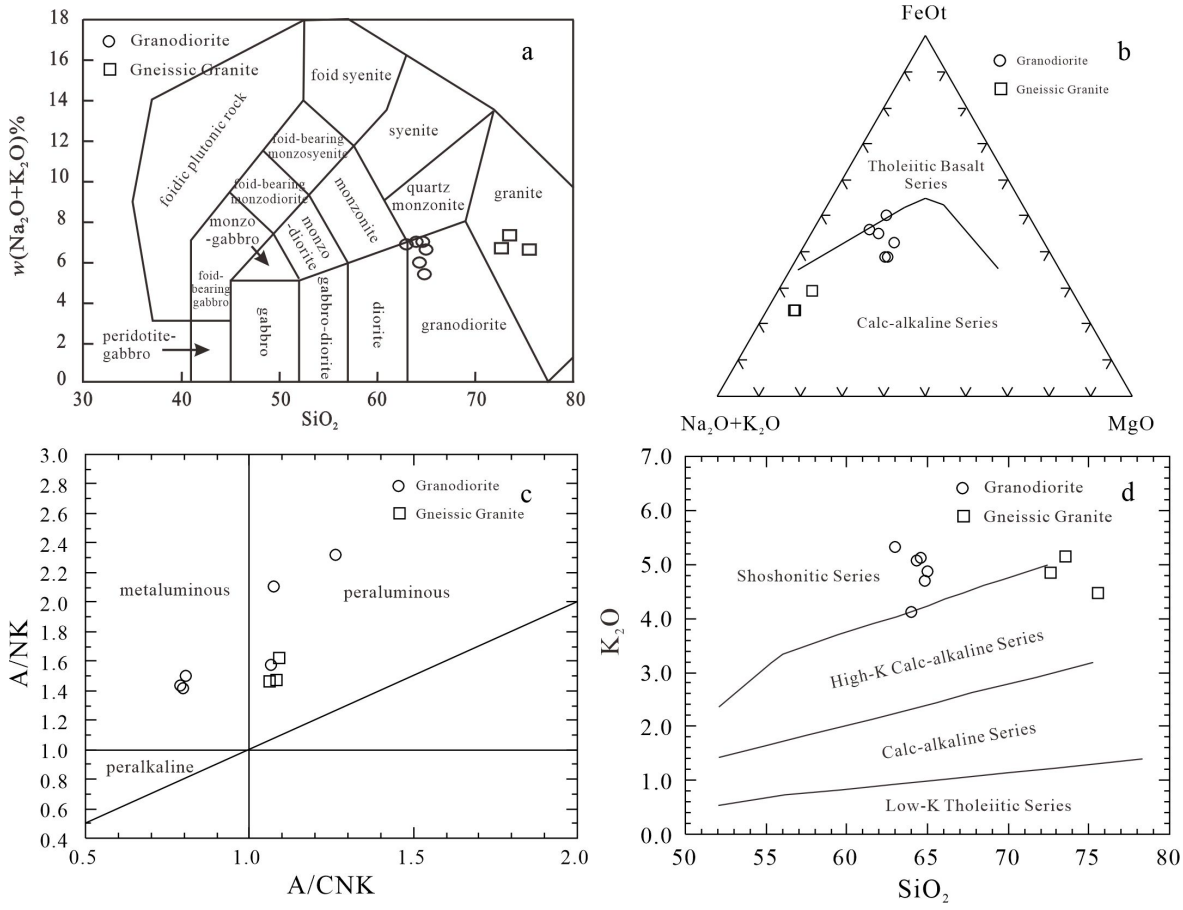

Figure 5. Various classification diagrams of intermediate–acidic intrusive rocks from the Wulanwuzhuer area ((**a**,**b**) after [45]; (**c**) after [46]; (**d**) after [47]).

The chondrite-normalized REE patterns (Figure 6a) indicate light REE (LREE) enrichment and low REEs contents, with (La/Yb)n ratios of 12.4–24.4 [48]. Furthermore, the samples exhibit significant negative Eu anomalies, with δEu values ranging from 0.25 to 0.61 (avg. 0.43). On the primitive mantle-normalized trace element spider diagram (Figure 6b), the samples are enriched in large-ion lithophile elements (LILEs) but depleted in high-field-strength elements (HFSEs) such as Nb, Ta, Ti, and P. The pronounced negative Eu anomalies, coupled with significant depletions in P and Ti, suggest the presence of residual mineral phases in the source region, such as plagioclase, apatite, amphibole, and ilmenite [49].

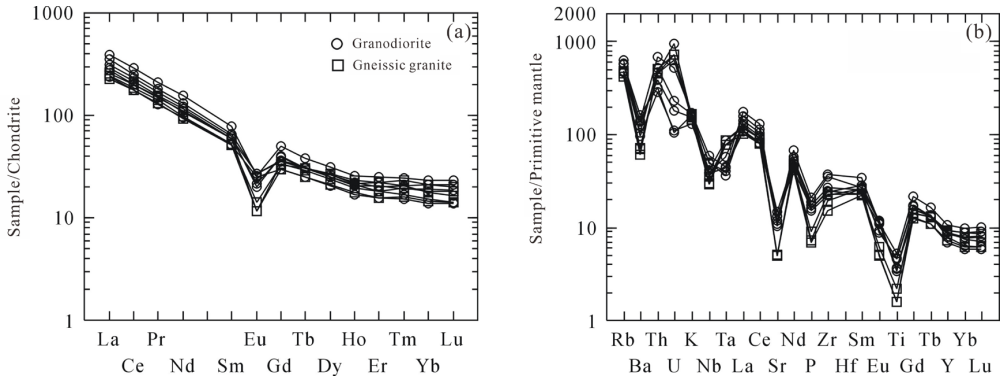

Figure 6. (**a**) Chondrite-normalized rare earth element patterns (chondrite standard values, after [45]) and (**b**) primitive mantle-normalized trace element patterns (primitive mantle standard values, after [50]) of intermediate–acidic intrusive rocks from the Wulanwuzhuer area.

5. Discussion

5.1. Formation Age

The formation age of this suite of intermediate–felsic intrusive rocks, which exhibits fault contact with the Qimantag Group in the Qimantag area, has been unclear. The Qinghai Institute of Geological Survey classified it as Hercynian during the 1:250,000-scale regional geological survey of the Kulangmiqiti Sheet in the western Qimantag tectono-magmatic belt [51]. The high-precision LA-ICP-MS zircon U-Pb age of 475.3 ± 2.0 Ma obtained in this study should represent the magmatic emplacement age of the intrusion. This age is comparable to the 486.4 ± 8.9 Ma SHRIMP zircon U-Pb age reported by Liu (2008) for the Wulan gneissic granite in the eastern segment of the East Kunlun Mountains [29]. Previous studies reported a crystallization age of 421.2 ± 1.9 Ma (MSWD = 2.1, n = 32) for the potassic granite adjacent to our sample location [14]. This age discrepancy may reflect that the pluton locally experienced a certain degree of metamorphism during the syn-collisional or post-collisional stage, resulting in the development of the gneissic structure observed in our samples.

The Nb-Ta-Ti depletions of the Wulanwuzhuer intermediate–felsic intrusion indicate an arc granite affinity associated with subduction.

In addition, trace element geochemistry of the Shizigou ophiolite in the Qimantag area shows characteristics of back-arc basin basalts. Its overall geochemical features are dominated by N-MORB-type signatures, with subordinate E-MORB affinities. Sm–Nd isochron dating indicates a Late Ordovician formation age of 442 ± 16 Ma (MSWD = 0.41, n = 9), suggesting that the ophiolite formed in a subduction-related back-arc basin setting [52], indicating the continued operation of subduction. The I-type granitoids in the EKOB, including the plutons in the Shuangshixia (461.7 ± 8.4 Ma, MSWD = 1.09, n = 23) [53], Annage (474.1 ± 2.4 Ma, MSWD = 0.32, n = 31) [54], Zhiyu (448 ± 2.5 Ma, MSWD = 0.16, n = 26) [55] and Bariqili (441 ± 6 Ma, MSWD = 0.76, n = 23) [56] areas from east to west, were generated from subduction-related tectonics. Furthermore, the discovery of a gabbro with a 444.5 ± 1.5 Ma Ar-Ar age associated with glaucophane schist southwest of Tumuleke in Qimantag [57], along with the identification of high-potassium adakitic rocks in the eastern East Kunlun, may mark the end of subduction and the beginning of syn-collision [58].

These data collectively indicate that the ages of arc granitoids in the East Kunlun region are primarily concentrated between 474 Ma and 441 Ma [23]. The ~475 Ma age obtained in this study for the gneissic biotite granite falls within this range, suggesting that it is a product of the early Caledonian orogeny, contemporaneous with the intrusions listed above. During the "1:50,000-scale regional geological survey project of the Wulanwuzhuer-Qimantag area" in Qinghai, Late Silurian peraluminous granite intrusions were identified north of the Wulanwuzhuer fault, yielding LA-ICP-MS zircon U-Pb ages of 438.7 ± 4.2 Ma (MSWD = 3.2, n = 7), which were interpreted to have formed in a syn-collisional setting [31]. This finding further supports the interpretation that the ~475 Ma granite south of this fault, as studied herein, represents a product of early Caledonian oceanic crust subduction.

5.2. Magma Source

Geochemical analysis reveals a marked consistency in the variation trends of major oxides and trace elements between the granodiorite and gneissic biotite granite. Their primitive mantle-normalized and chondrite-normalized trace element patterns are broadly similar, indicative of a comagmatic evolutionary relationship. This suggests that both rock types share a common magmatic origin and formed in a consistent tectonic setting.

The Wulanwuzhuer intermediate–felsic intrusion exhibits high total alkali contents ($K_2O + Na_2O$ = 5.32%–7.22%), alongside low MgO (0.67%–3.96%), low $Mg^{\#}$ values (33–50), and low Ni concentrations (2.80–15.8 × 10^{-6}). These geochemical characteristics suggest

derivation from partial melting of lower crustal material. This interpretation is supported by the fact that partial melting of mantle peridotite cannot yield magmas more felsic than andesite or boninite (SiO_2 < 55%) [59]. Thus, the magma is unlikely to originate directly from mantle peridotite but rather from partial melting of a mafic lower crustal source. Furthermore, the samples show Rb/Sr ratios (0.95–2.84) approximating the average continental crust value (0.35; [60]), while their Ti/Zr (9.55–19.8) and Ti/Y (53.7–152) ratios fall within ranges typical of crust-derived rocks (Ti/Zr < 30, Ti/Y < 200; [61]), showing crustal geochemical features.

Xiao et al. (2005) [62] noted that within the East Kunlun Orogenic Belt, early Caledonian (480–490 Ma) granitoids with positive $\varepsilon_{Nd}(t)$ values occur during the initial orogenic phase, while negative $\varepsilon_{Nd}(t)$ values are observed in granitoids from other orogens formed by oceanic subduction, such as the Qinling-Dabie [63] and the Gangdese belt in the Tibetan Plateau [64]. The high K_2O contents of granitoids further indicate that the island arc formed by subducting oceanic crust during this period was a mature arc underlain by continental crust. Experimental studies in the K_2O-MgO-Al_2O_3-SiO_2-H_2O (KMASH) system by Massonne (1992) demonstrated that minor potassium-rich metasediments within subducted oceanic crust can generate ultra-potassic fluids under conditions of 300–600 °C and 15–30 kbar (1 bar = 100 kPa) [65]. During ascent, these fluids infiltrate the overlying mantle, inducing metasomatism and forming an enriched mantle wedge. Subsequent thermal events may trigger partial melting of this metasomatized mantle, producing potassium-rich magmas underplating and forming lower crust, serving as the source region for these granites—a plausible mechanism for the high potassium contents observed in the studied rocks.

In summary, the magma source of the Wulanwuzhuer intermediate–felsic intrusion is attributed to the partial melting of lower crust, which had undergone metasomatism by fluids derived from the subducted oceanic crust and then experienced mixing and homogenization of crustal melts.

5.3. Tectonic Setting

The existing research indicates that shoshonitic series rocks primarily originate by potassium- and large-ion lithophile element (LILE)-enriched mantle metasomatism related to subduction processes. They typically develop in oceanic island arcs during later stages of subduction, spatially distant from the trench, and can also form abundantly in continental arc and post-collisional arc settings. Only a very small proportion occur in intraplate rift or passive continental margin environments [66–68]. On the La-P_2O_5 and La/Nb vs. Ba/Nb tectonic discrimination diagrams (Figure 6a,b), all samples plot within the field of arc volcanism. On the Ta/Yb vs. Th/Yb diagram (Figure 7), the samples more specifically indicate an active continental margin tectonic setting, suggesting that the intrusion formed in a subduction-related environment along an active continental margin. On the R1–R2 tectonic discrimination diagram (Figure 7), the samples primarily fall within the pre-plate collision field, corresponding to an active plate margin, and show a trend evolving towards the syn-collisional granite field.

The Kunlun region was characterized by a continuous compressional orogenic tectonic setting during the Caledonian period [69–71]. Several lines of evidence indicate that the East Kunlun had evolved from a passive continental margin to an active continental margin involving oceanic crust subduction by the Caledonian period. These include the predominance of pre-collisional and syn-collisional granitoids among the early Caledonian granites in the East Kunlun, and the formation of the Early Paleozoic Tanjianshan Group (Qimantag Group) bimodal volcanic rocks in the North Kunlun belt [9]. Bai et al. (2001) [27], summarizing Caledonian granitoids in the eastern East Kunlun, proposed that the Early

Ordovician arc granites formed in a subduction-related geodynamic setting. Mo et al. (2007) [23] suggested that the eastern East Kunlun entered a subduction stage starting in the Middle Cambrian, which persisted until the Late Ordovician. Zhang et al. (2010) [72], based on geochronological studies of the Dulan Kekesha quartz diorite in the East Kunlun orogen, concluded that its formation age of 515.2 ± 4.4 Ma represents the initial stage of oceanic basin subduction. Significant rifting occurred in the Qimantag area during the Early Ordovician, with local zones potentially developing into small oceanic basins [3,11]. The discovery of Early Ordovician island-arc type diorite in the Yaziquan area of Qimantag by Cui et al. (2011) [73] further indicates that the Qimantag Ocean already existed prior to the Early Ordovician and was undergoing northward-directed subduction (subduction polarity likely from south to north) during that time [74–76]. Integrating the findings of this study, we propose that the Wulanwuzhuer intermediate–felsic intrusion formed in an active continental margin tectonic setting during the early Caledonian. This setting involved the initiation of northward subduction of the Proto-Tethyan oceanic crust (including the Qimantag Ocean and the Central East Kunlun Ocean) beneath the Qaidam Block along the vicinity of the present-day Central Kunlun Fault.

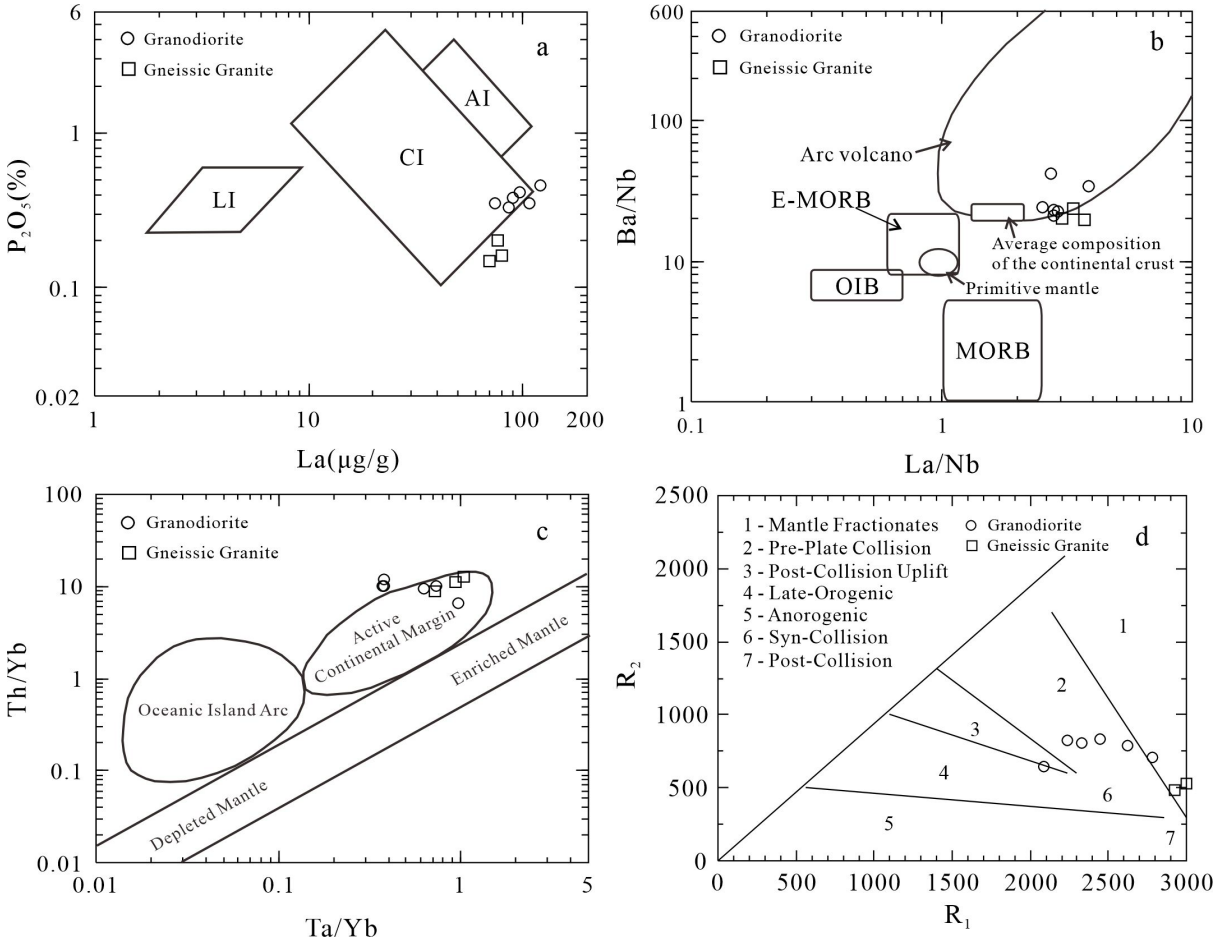

Figure 7. Tectonic setting discrimination diagrams of intermediate–acidic intrusive rocks from the Wulanwuzhuer area ((**a**) after [77]; (**b**) after [78]; (**c**) after [79]; (**d**) after [80]). AI—Andean-type; CI—continental island arc and oceanic island arc type; LI—low-K andesite of oceanic island arc type.

6. Conclusions

1. Zircon U-Pb dating of the Wulanwuzhuer gneissic biotite granite yields a weighted mean age of 475.3 ± 2.0 Ma. These results indicate that the intrusion formed during the Caledonian period, rather than the Hercynian period as previously suggested.

2. The magmas that formed the Wulanwuzhuer intermediate–felsic intrusion were derived primarily from partial melting of lower crust, which had undergone metasomatism by fluids derived from a subducted oceanic slab.
3. This suite of intermediate–felsic intrusive rocks formed in an active continental margin setting during the early Caledonian. This tectonic environment was characterized by the initiation of northward subduction of the Proto-Tethyan oceanic crust beneath the Qaidam block along the vicinity of the present-day Central Kunlun Fault.

Supplementary Materials: The following supporting information can be downloaded at: https://www.mdpi.com/article/10.3390/min16030272/s1, Supplementary Data Table S1: Early Paleozoic magmatic, metamorphic, sedimentary records of the EKOB. References [51,53,81–101] are cited in the Supplementary Materials.

Author Contributions: Conceptualization, M.A. and J.Z.; methodology, Q.X.; software, Y.Y.; validation, Z.D.; formal analysis, G.M. All authors have read and agreed to the published version of the manuscript.

Funding: This research was funded by the Science and Technology Support Project for the New Round of Strategic Action to Find Mineral Breakthroughs (No. ZKKJ202406), the National Natural Science Foundation of China (U22A20571, 42172087), and the Shandong Provincial Natural Science Foundation of China (ZR2019PD017, ZR2021QD086).

Data Availability Statement: The original contributions presented in this study are included in the article/Supplementary Material. Further inquiries can be directed to the corresponding author.

Acknowledgments: Zircon separation was carried out at the Laboratory of the Langfang Regional Geological Survey Institute, Hebei Province. Cathodoluminescence (CL) imaging and LA-ICP-MS U–Pb zircon dating were performed at the State Key Laboratory of Continental Dynamics, Northwest University. Whole-rock major and trace element analyses were conducted at the Center of Test Science, Jilin University. The authors sincerely thank these laboratories for their technical support and assistance during sample preparation, analytical procedures, and data processing. The authors also gratefully acknowledge the editor and anonymous reviewers for their constructive comments and valuable suggestions, which significantly improved the quality and clarity of this manuscript.

Conflicts of Interest: The authors declare no conflicts of interest.

References

1. Xin, W.; Sun, F.Y.; Zhang, Y.T.; Fan, X.Z.; Wang, Y.C.; Li, L. Mafic–intermediate igneous rocks in the East Kunlun Orogenic Belt, northwestern China: Petrogenesis and implications for regional geodynamic evolution during the Triassic. *Lithos* **2019**, *346*, 105159. [CrossRef]
2. Xin, W.; Ding, Z.J.; Meng, Y.K.; Bo, J.W.; Li, L.; Mao, G.Z. Late Triassic granites with mafic microenclaves in the East Kunlun Orogenic Belt, northwestern China: Petrogenesis and implications for continental crust evolution and geodynamic evolution. *Can. J. Earth Sci.* **2023**, *60*, 672–691. [CrossRef]
3. Miao, T.; Zhao, X.; Huizenga, J.M.; Li, X.; Lai, L.; Li, B.; Wei, J. Segmented Paleo-Tethys subduction and its role in driving Triassic magmatism within the Elashan Tectonic–Magmatic Belt, northern Tibetan Plateau. *Lithos* **2025**, *522-523*, 108387. [CrossRef]
4. Dong, Y.; Sun, S.; Santosh, M.; Zhao, J.; Sun, J.; He, D.; Zhang, G. Central China orogenic belt and amalgamation of East Asian continents. *Gondwana Res.* **2021**, *100*, 131–194. [CrossRef]
5. Dong, Y.; Sun, S.; Santosh, M.; Hui, B.; Sun, J.; Zhang, F.; Qi, N. Cross orogenic belts in Central China: Implications for the tectonic and paleogeographic evolution of the East Asian continental collage. *Gondwana Res.* **2022**, *109*, 18–88. [CrossRef]
6. Wu, J.J.; Yang, J.Z.; Zeng, Q.D.; Fan, H.R.; Frimmel, H.E.; Yang, K.F.; Li, X.H.; Liang, G.Z. Two distinct tectono–magmatic episodes and associated gold mineralization in the Wulonggou gold district, East Kunlun Orogenic Belt. *Gondwana Res.* **2026**, *150*, 312–334. [CrossRef]
7. Sun, F.Y.; Chen, G.H.; Chi, X.G.; Li, B.L.; Zhao, J.W. *Comprehensive Study on Metallogenic Regularity and Prospecting Direction of the East Kunlun Metallogenic Belt in Qinghai, Xinjiang*; Research Report of Geological Survey Project; China Geological Survey: Beijing, China, 2003.

8. Wang, M.; Pei, X.Z.; Pei, L.; Li, R.B.; Li, Z.C.; Liu, C.J.; Chen, Y.X.; Hu, N.; Qin, L.; Wang, X. Multi-stage tectono–magmatic evolution of the Proto-Tethys Ocean: Constraints from Mid-Paleozoic granitoids in the East Kunlun–North Qaidam orogenic belt. *Gondwana Res.* **2026**, *150*, 82–108. [CrossRef]
9. Wang, X.; Ding, L.; Wang, C.; Zeng, D.; Wang, Z.; Yang, L.; Xie, J. Proterozoic tectonic affinity and evolution of the East Kunlun–Qaidam Block, NW China: Insight from Precambrian metasedimentary rocks and early Neoproterozoic granitoids. *Precambrian Res.* **2024**, *409*, 107451. [CrossRef]
10. Liu, X.; Lü, Z.; Chen, Z.; Song, S.; Guo, Y. Metamorphic evolution and tectonic significance of garnet-bearing amphibolites from the upper valley of the Hatu River, East Kunlun Orogenic Belt. *Lithos* **2025**, *504*, 108027. [CrossRef]
11. Zhang, M.; Tan, S.; Ruan, M.; Li, L.; Yan, Q. Petrogenesis and tectonic implication of the Triassic monzogranite from the central segment of the East Kunlun Orogen, NW China. *J. Asian Earth Sci.* **2024**, *276*, 106341. [CrossRef]
12. Xin, W.; Sun, F.Y.; Li, L.; Yan, J.M.; Zhang, Y.T.; Wang, Y.C.; Yang, Y.J. The Wulonggou metaluminous A2-type granites in the Eastern Kunlun Orogenic Belt, NW China: Rejuvenation of subduction-related felsic crust and implications for post-collision extension. *Lithos* **2018**, *312*, 108–127. [CrossRef]
13. Yan, D.; Zhou, H.; Li, C.; Zhang, X.; Ma, C.; Hou, M.; Xiong, F. Petrogenesis of Late Triassic adakitic plutons in the East Kunlun Orogen, Northern Tibet: Geodynamic implications for the Paleo-Tethyan orogeny and crustal evolution. *J. Asian Earth Sci.* **2024**, *268*, 106165. [CrossRef]
14. Hao, N.N.; Yuan, W.; Zhang, A.; Feng, Y.; Cao, J.; Chen, X.; Mo, X. Evolution process of the Late Silurian–Late Devonian tectonic environment in Qimantagh in the western portion of east Kunlun, China: Evidence from the geochronology and geochemistry of granitoids. *J. Earth Syst. Sci.* **2015**, *124*, 171–196. [CrossRef]
15. Zhong, S.; Li, S.; Feng, C.; Liu, Y.; Santosh, M.; He, S.; Zhou, J. Porphyry copper and skarn fertility of the northern Qinghai–Tibet Plateau collisional granitoids. *Earth-Sci. Rev.* **2021**, *214*, 103524. [CrossRef]
16. Chen, Y.C.; Ding, Z.J.; Bo, J.W.; Han, S.J.; Li, T.T.; Ji, P.; Guo, R.Q. Petrogenesis and age of granitoids associated with the Dongshan Cu polymetallic deposit, East Kunlun Orogenic Belt, NW China: Implications for the Middle to Late Triassic tectonic setting and Cu polymetallic mineralization. *Geochemistry* **2025**, *85*, 126240. [CrossRef]
17. Zhao, Z.X.; Dong, G.C.; Santosh, M.; Zhu, D.C.; Kong, H.L.; Lü, S.J.; Zhong, P.Y. The mafic–ultramafic roots of a magmatic arc from the East Kunlun Orogen, NW China. *Gondwana Research* **2025**, *143*, 142–156. [CrossRef]
18. Shao, F.; Niu, Y.; Kong, J.; Liu, Y.; Wang, G.; Zhang, Y. Petrogenesis and tectonic implications of the Triassic rhyolites in the East Kunlun Orogenic Belt, northern Tibetan Plateau. *Geosci. Front.* **2021**, *12*, 101243. [CrossRef]
19. Li, X.; Huang, X.; Luo, M.; Dong, G.; Mo, X. Petrogenesis and geodynamic implications of the Mid-Triassic lavas from East Kunlun, northern Tibetan Plateau. *J. Asian Earth Sci.* **2015**, *105*, 32–47. [CrossRef]
20. Kong, J.; Niu, Y.; Hu, Y.; Zhang, Y.; Shao, F. Petrogenesis of the Triassic granitoids from the East Kunlun Orogenic Belt, NW China: Implications for continental crust growth from syn-collisional to post-collisional setting. *Lithos* **2020**, *364*, 105513. [CrossRef]
21. Zhou, H.; Zhang, D.; Wei, J.; Wang, D.; Santosh, M.; Shi, W.; Zhao, X. Petrogenesis of Late Triassic mafic enclaves and host granodiorite in the Eastern Kunlun Orogenic Belt, China: Implications for the reworking of juvenile crust by delamination-induced asthenosphere upwelling. *Gondwana Res.* **2020**, *84*, 52–70. [CrossRef]
22. Xia, R.; Wang, C.; Deng, J.; Carranza, E.J.M.; Li, W.; Qing, M. Crustal thickening prior to 220 Ma in the East Kunlun Orogenic Belt: Insights from the Late Triassic granitoids in the Xiao–Nuomuhong pluton. *J. Asian Earth Sci.* **2014**, *93*, 193–210. [CrossRef]
23. Shao, F.; Niu, Y.; Liu, Y.; Chen, S.; Kong, J.; Duan, M. Petrogenesis of Triassic granitoids in the East Kunlun Orogenic Belt, northern Tibetan Plateau and their tectonic implications. *Lithos* **2017**, *282*, 33–44. [CrossRef]
24. Liu, B.; Ma, C.Q.; Huang, J.; Wang, L.X.; Zhao, S.Q.; Yan, R.; Xiong, F.H. Petrogenesis and tectonic implications of Upper Triassic appinite dykes in the East Kunlun orogenic belt, northern Tibetan Plateau. *Lithos* **2017**, *284*, 766–778. [CrossRef]
25. Hu, Y.; Niu, Y.; Li, J.; Ye, L.; Kong, J.; Chen, S.; Zhang, G. Petrogenesis and tectonic significance of the Late Triassic mafic dikes and felsic volcanic rocks in the East Kunlun Orogenic Belt, northern Tibetan Plateau. *Lithos* **2016**, *245*, 205–222. [CrossRef]
26. Qu, H.; Friehauf, K.; Santosh, M.; Pei, R.; Li, D.; Liu, J.; Wang, H. Middle–Late Triassic magmatism in the Hutouya Fe–Cu–Pb–Zn deposit, East Kunlun Orogenic Belt, NW China: Implications for geodynamic setting and polymetallic mineralization. *Ore Geol. Rev.* **2019**, *113*, 103088. [CrossRef]
27. Bai, Y.S.; Chang, G.H.; Tan, S.X.; Wang, J.S. Study on The Features of Caledonian Intrusive Rocks in the Eastern Sector of East Kunlun. *Geol. Qinghai* **2001**, *9*, 28–35. (In Chinese with English abstract)
28. Zhao, Z.M.; Ma, H.D.; Wang, B.Z.; Bai, Y.S.; Li, R.S.; Ji, W.H. The Evidence of Intrusive Rocks about Collision-orogenyduring Early Devonian in Eastern Kunlun Area. *Geol. Rev.* **2008**, *54*, 47–56. (In Chinese with English abstract)
29. Liu, C.D. *Granitoid Magma Mixing in Eastern Part of the East Kunlun Orogenic Belt*; Geological Publishing House: Beijing, China, 2008; pp. 21–28. (In Chinese)
30. Qiao, G.B.; Wu, Y.Z. Genetic Types of Granite Controlled the Mineralization in Qimantag Area, Eastern Kunlun. *Northwestern Geol.* **2010**, *43*, 134–142. (In Chinese with English abstract)

31. Tan, S.X.; Guo, T.Z.; Dong, J.S.; Chang, Y.Y.; Ma, W. Geological Characteristics and Significance of the Peraluminous Granite in Late Silurian Epoch in Wulanrvuzhuer Region of Qinghai. *J. Qinghai Univ. Nat. Sci. Ed.* **2011**, *29*, 36–43. (In Chinese with English abstract)
32. Guo, T.Z.; Liu, R.; Chen, F.B.; Bai, X.D.; Li, H.G. LA-MC-ICPMS zircon U-Pb Dating of Wulanwuzhuer Porphyritic Syenite Granite in the Qimantag Mountain of Qinghai and its Geological significance. *Geol. Bull. China* **2011**, *30*, 1203–1211. (In Chinese with English abstract)
33. Cao, S.T.; Liu, X.K.; Ma, Y.S.; Li, J.Y.; Ma, Y.L. Discovery of the Early Silurian intrusive rocks in the Qimantag and its geological significance. *Qinghai Sci. Technol.* **2011**, *5*, 26–30.
34. Hu, J.; Wang, H.; Wang, M. Geochemistry and origin of the Neoproterozoic Dahongliutan banded iron formation (BIF) in the Western Kunlun orogenic belt, Xinjiang (NW China). *Ore Geol. Rev.* **2017**, *89*, 836–857. [CrossRef]
35. Dong, Y.P.; He, D.F.; Sun, S.S.; Liu, X.M.; Zhou, X.H.; Zhang, F.F.; Yang, Z.; Cheng, B.; Zhao, G.C.; Li, J.H. Subduction and accretionary tectonics of the East Kunlun orogen, western segment of the Central China Orogenic System. *Earth Sci. Rev.* **2018**, *186*, 231–261. [CrossRef]
36. Han, Z.H.; Sun, F.Y.; Tian, N.; Gao, H.C.; Li, L.; Zhao, T.F. Zircon U-Pb Geochronology, Geochemistry and Geological lmplicationsof the Early Paleozoic Wulanwuzhuer Granites in the Qimantag, EastKunlun, China. *Earth Sci.* **2021**, *46*, 13–30. (In Chinese with English abstract)
37. Andersen, T. Correction of Common Lead in U-Pb Analyses that do not Report 204Pb. *Chem. Geol.* **2002**, *192*, 59–79. [CrossRef]
38. Ludwig, K.R. *Users Manual for Isoplot/Ex, Version 3.00, A Geochronological Toolkit for Microsoft Excel*; Special Publication No. 4; Berkeley Geochronology Centre: Berkeley, CA, USA, 2003.
39. Yuan, H.L.; Gao, S.; Liu, X.M.; Li, H.M.; Günther, D.; Wu, F.Y. Accurate U-Pb Age and Trace Element Determinations of Zircon by Laser Ablation Inductively Coupled Plasma-mass Spectrometry. *Geostand. Geoanal. Res.* **2004**, *28*, 357–370. [CrossRef]
40. Liu, X.M.; Gao, S.; Diwu, C.R.; Yuan, H.L.; Hu, Z.C. Simultaneous in-situ Determination of U-Pb Age and Trace Elements in Zircon. *Chin. Sci. Bull.* **2007**, *52*, 228–235. (In Chinese with English abstract)
41. *GB/T 14506.28-93*; Methods for Chemical Analysis of Silicate Rocks—Part 28: Determination of Lead. Standards Press of China: Beijing, China, 1993.
42. *DZ/T 0223-2001*; General Rule for Inductively Coupled Plasma Massspectrometry (ICP-MS) Analytical Method. Standards Press of China: Beijing, China, 2002.
43. *GBW07103*; Standard Reference Material for Rock Composition Analysis: Granite. Standards Press of China: Beijing, China, 2015.
44. *GBW07104*; Standard Reference Material for Rock Composition Analysis: Andesite. Standards Press of China: Beijing, China, 2015.
45. Irvine, T.H.; Baragar, W.R.A. A Guide to the Chemical Classification of the Common Volcanic rocks. *Can. J. Earth Sci.* **1971**, *8*, 523–548. [CrossRef]
46. Maniar, P.D.; Piccoli, P.M. Tectonic Discrimination of Granitoids. *Geol. Soc. Am. Bull.* **1989**, *101*, 635–643. [CrossRef]
47. Rickwood, P.C. Boundary Lines within Petrologic Diagrams which Use Oxides of Major and Minor Elements. *Lithos* **1989**, *22*, 247–263. [CrossRef]
48. Boynton, W.V. Geochemistry of the Rate Earth Elements: Meteorite studies. In *Rare Earth Elements Geochemistry*; Henderson, P., Ed.; Elsevier: Amsterdam, The Netherlands, 1984; pp. 63–114.
49. Lightfoot, P.C.; Hawkesworth, C.J.; Sethna, S.F. Petrogenesis of Rhyolites and Trachytes from the Deccan Trap: Sr, Nd and Pb Isotope and Trace Element Evidence. *Contrib. Mineral. Petrol.* **1987**, *95*, 44–54. [CrossRef]
50. Sun, S.S.; McDonough, W.F. Chemical and Isotopic Systematics of Oceanic Basalts: Implications for Mantle Composition and Processes. *Spec. Publ. Geol. Soc. Lond.* **1989**, *42*, 313–345. [CrossRef]
51. Qinghai Institute of Geological Survey. *1,250,000 Scale Regional Geological Survey Report of the Kulangmiqiti Sheet*; Qinghai Institute of Geological Survey: Xining, China, 2003.
52. Song, T.Z.; Zhao, H.X.; Zhang, W.K.; Bai, X.D.; An, S.W.; Yang, M. The geological features of Shizigou ophiolites in Qimantage Area. *Northwestern Geol.* **2010**, *43*, 124–133. (In Chinese with English abstract)
53. Li, W.; Neubauer, F.; Liu, Y.J.; Genser, J.; Ren, S.M.; Han, G.Q.; Liang, C.Y. Paleozoic evolution of the Qimantagh magmatic arcs, Eastern Kunlun Mountains: Constraints from zircon dating of granitoids and modern river sands. *J. Asian Earth Sci.* **2013**, *77*, 183–202. [CrossRef]
54. Kong, H.L.; Li, J.C.; Li, Y.Z.; Jia, Q.Z.; Yang, B.R. Geochemistry and zircon U–Pb geochronology of the Annage diorite in the eastern section of the East Kunlun, Qinghai Province. *Geol. Sci. Technol. Inf.* **2014**, *33*, 11–17. (In Chinese with English abstract)
55. Zhou, B.; Dong, Y.P.; Zhang, F.F.; Yang, Z.; Sun, S.S.; He, D.F. Geochemistry and zircon U–Pb geochronology of granitoids in the East Kunlun Orogenic Belt, northern Tibetan Plateau: Origin and tectonic implications. *J. Asian Earth Sci.* **2016**, *130*, 265–281. [CrossRef]

56. Liu, Z.Q.; Pei, X.Z.; Li, R.B.; Li, Z.C.; Chen, G.C.; Chen, Y.X.; Gao, J.M.; Liu, C.J.; Wei, F.H.; Wang, X.L.; et al. Early Paleozoic intermediate–acid magmatic activity in the Bairiqiete area along the Buqingshan tectonic mélange belt on the southern margin of the East Kunlun: Constraints from zircon U–Pb dating and geochemistry. *Geol. China* **2011**, *38*, 1150–1167. (In Chinese with English abstract)
57. Qinghai Institute of Geological Survey. *1,250,000 Scale Regional Geological Survey Report of the Bukadaban Feng Sheet*; Qinghai Institute of Geological Survey: Xining, China, 2003.
58. Liu, B.; Ma, C.Q.; Zhang, J.Y.; Xiong, F.H.; Huang, J.; Jiang, H.A. Petrogenesis of Early Devonian intrusive rocks in the east part of Eastern Kunlun Orogen and implication for Early Palaeozoic orogenic proceses. *Acta Petrol. Sin.* **2012**, *28*, 1785–1807.
59. Baker, M.B.; Hirschmann, M.M.; Ghiorso, M.S.; Stolper, E.M. Compositions of near-solidus peridotite melts from experiments and thermodynamic calculations. *Nature* **1995**, *375*, 308–311. [CrossRef]
60. Taylor, S.R.; McLennan, S.M. The geochemical evolution of the continental crust. *Rev. Geophys.* **1995**, *33*, 241–265. [CrossRef]
61. Wedepohl, K.H. The composition of the continental crust. *Geochim. Cosmochim. Acta* **1995**, *59*, 1217–1232. [CrossRef]
62. Xiao, Q.H.; Qiu, R.Z.; Deng, J.F.; Li, T.D.; Mo, X.X.; Hong, D.W.; Lu, X.X.; Wang, T.; Wu, F.Y.; Xie, C.F. Granitoids and Continental Crustal Growth Modes in China. *Geol. China* **2005**, *32*, 343–352. (In Chinese with English abstract)
63. Hong, D.W.; Wang, T.; Tong, Y.; Wang, X.X. Mesozoic Granitoids from North China Block and Qinling-Dabie-Sulu Orogenic Belt and their Deep Dynamic Process. *Earth Sci. Front.* **2003**, *10*, 231–256. (In Chinese with English abstract)
64. Qiu, R.Z.; Deng, J.F.; Zhou, S.; Xiao, Q.H.; Cai, Z.Y.; Liu, C. Study on Sr-Nd Isotopes of Mesozoic-Cenozoic Granites in Qinghai-Tibetan Plateau. *Acta Geosci. Sin.* **2003**, *24*, 611–617. (In Chinese with English abstract)
65. Massonne, H.J. Evidence for low-temperature ultrapotassic siliceous fluids in subduction zone environments from experiments in the system K_2O-MgO-Al_2O_3-SiO_2-H_2O (KMASH). *Lithos* **1992**, *28*, 421–434. [CrossRef]
66. Morrison, G.W. Characteristics and Tectonic Setting of the Shoshonite Rock Association. *Lithos* **1980**, *13*, 91–108. [CrossRef]
67. Foley, S.F.; Peccerillo, A. Potassic and Ultrapotassic Magmas and their Origin. *Lithos* **1992**, *28*, 181–185. [CrossRef]
68. Müller, D.; Groves, D.I. *Potassic Igneous Rocks and Associated Gold-Copper Mineralization*; Springer: Berlin/Heidelberg, Germany, 1995; pp. 1–210.
69. Pan, Y.S. Tectonic Features and Evolution of the Western Kunlun Mountain Region. *Sci. Geol. Sin.* **1990**, *25*, 224–232. (In Chinese with English abstract)
70. Pan, Y.S. Geological Features and Tectonic Evolution of Geotraverse from Yecheng to Shiquanhe in the Tibetan plateau. *Acta Geol. Sin.* **1994**, *68*, 295–307. (In Chinese with English abstract)
71. Şengör, A.M.C.; Okurogullari, A.H. The Role of Accretionary Wedges in the Growth of Continents: Asiatic Examples from Argand to Plate Tectonics. *Eclogae Geol. Helv.* **1991**, *84*, 535–597.
72. Zhang, Y.F.; Pei, X.Z.; Ding, S.P.; Li, R.B.; Feng, J.Y.; Sun, Y.; Li, Z.C.; Chen, Y.X. LA-ICP-MS Zircon U-Pb Age of Quartz Diorite at the Kekesha Area of Dulan County, Eastern Section of the East Kunlun Orogenic Belt, China and its Significance. *Geol. Bull. China* **2010**, *29*, 79–85. (In Chinese with English abstract)
73. Cui, M.H.; Meng, F.C.; Wu, X.K. Early Ordovician Island Arc of Qimantag Mountain, Eastern Kunlun: Evidences from Geochemistry, Sm-Nd Isotope and Geochronology of Intermediate-basic Igneous Rocks. *Acta Petrol. Sin.* **2011**, *27*, 3365–3379. (In Chinese with English abstract)
74. Wang, Y.J.; Shen, Y.C.; Lin, G. Preliminary Research on the Tectonostratigraphy in the Northern Central-Kunlun Orogenic Belt. *J. Stratigr.* **2000**, *24*, 55–59. (In Chinese with English abstract)
75. Li, D.P.; Li, J.; Zhang, H.J.; Li, X.L.; Zhou, X.K.; Du, S.X. The Turbidite of the Silurian Baiganhu Formation in the Qimantag Mountain Eastern Kunlun. *Geol. Shaanxi* **2003**, *21*, 39–44. (In Chinese with English abstract)
76. Chen, J.L.; Li, D.P.; Li, X.L.; Zhou, X.K.; Wang, X.L.; Wang, X.X.; Dai, X.Y.; Du, S.X.; Gao, X.P. The Discovery and Features of the Heishan Ophiolite in the South Margin of Qimantag Mountain, Eastern Kunlun. *Geol. Shaanxi* **2004**, *22*, 35–46. (In Chinese with English abstract)
77. Bailey, J.C. Geochemical Criteria for a Refined Tectonic Discrimination of Orogenic Andesites. *Chem. Geol.* **1981**, *32*, 139–154. [CrossRef]
78. Jahn, B.M.; Wu, F.Y.; Lo, C.H. Crust—Mantle Interaction Induced by Deep Subduction of the Continental Crust: Geochemical and Sr-Nd Isotopic Evidence from Post-collisional Mafic—Ultramafic Intrusions of the Northern Dabie Complex, Central China. *Chem. Geol.* **1999**, *157*, 119–146. [CrossRef]
79. Pearce, J.A. Role of the sub-continental lithosphere in magma genesis at active continental margins. In *Continental Basalts and Mantle Xenoliths*; Hawkesworth, C.J., Norry, M.J., Eds.; Shiva Publications: Nantwich, UK, 1983; pp. 230–249.
80. Batchelor, R.A.; Bowden, P. Petrogenetic Interpretation of Granitoid Rock Series Using Multi-cationic Parameters. *Chem. Geol.* **1985**, *48*, 43–55. [CrossRef]
81. Feng, C.Y.; Zhang, D.Q.; Dang, X.Y.; Li, D.X.; She, H.Q. SHRIMP zircon U-Pb dating of quartz albitite from the Tuolugou cobalt (gold) deposit, Golmud, Qinghai, China—Constraints on the age of the Naij Tal Group. *Geol. Bull. China* **2005**, *24*, 501–505. (In Chinese with English abstract)

82. He, D.F.; Dong, Y.P.; Liu, X.M.; Yang, Z.; Sun, S.S.; Cheng, B.; Li, W. Tectono-thermal events in East Kunlun, Northern Tibetan Plateau: Evidence from zircon U-Pb geochronology. *Gondwana Res.* **2016**, *30*, 179–190. [CrossRef]
83. Jiang, C.Y.; Ling, J.L.; Zhou, W.; Du, W.; Wang, Z.X.; Fan, Y.Z.; Song, Y.F.; Song, Z.B. Petrogenesis of the Xiarihamu Ni-bearing layered mafic-ultramafic intrusion, East Kunlun: Implications for its extensional island arc environment. *Acta Petrol. Sin.* **2015**, *31*, 1117–1136. (In Chinese with English abstract)
84. Li, H.K.; Lu, S.N.; Xiang, Z.Q.; Zhou, H.Y.; Guo, H.; Song, B.; Zheng, J.K.; Gu, Y. SHRIMP U-Pb zircon age of the granulite from the Qingshuiquan area, Central Eastern Kunlun Suture Zone. *Front. Earth Sci.* **2006**, *13*, 311–321. (In Chinese with English abstract)
85. Li, R.S.; Ji, W.H.; Yang, Y.C.; Yu, P.S.; Zhao, Z.M.; Chen, S.J.; Meng, Y.; Pan, X.P.; Shi, B.D.; Zhang, W.J.; et al. *Kunlun Mountains and Geology of Adjacent Areas*; Geological Publishing House: Beijing, China, 2008; pp. 1–400. (In Chinese with English abstract)
86. Li, X.; Yuan, W.M.; Hao, N.N.; Duan, H.W.; Chen, X.N.; Mo, X.X.; Zhang, A.K. Characteristics and tectonic setting of granite in Wulonggou area, East Kunlun Mountains. *Global Geol.* **2014**, *33*, 275–289. (In Chinese with English abstract)
87. Qi, S.S. Petrotectonic Assemblages and Tectonic Evolution of the East Kunlun Orogenic Belt in Qinghai Province. Doctoral Dissertation, China University of Geosciences, Beijing, China, 2015. (In Chinese with English abstract)
88. Qi, S.S.; Song, S.G.; Shi, L.C.; Cai, H.J.; Hu, J.C. Discovery and its geological significance of early Paleozoic eclogite in Xiarihamu-Suhaitu area, western part of the East Kunlun. *Acta Petrol. Sin.* **2014**, *30*, 3345–3356. (In Chinese with English abstract)
89. Qi, X.P.; Yang, J.; Fan, X.G.; Cui, J.T.; Cai, Z.F.; Zeng, X.W.; Wei, W.; Qu, X.X.; Zhai, L.M. Age, geochemical characteristics and tectonic significance of Changshishan ophiolite in central East Kunlun tectonic melange belt along the east section of East Kunlun Mountains. *Geol. China* **2016**, *43*, 797–816. (In Chinese with English abstract)
90. Qi, X.P.; Fan, X.G.; Yang, J.; Cui, J.T.; Wang, B.Y.; Fan, Y.Z.; Yang, G.X.; Li, Z.; Chao, W.D. The discovery of Early Paleozoic eclogite in the upper reaches of Langmuri in eastern East Kunlun Mountains and its significance. *Geol. Bull. China* **2016**, *35*, 1771–1783.
91. Ren, J.H.; Liu, Y.Q.; Feng, Q.; Han, W.Z.; Gao, H.; Zhou, D.W. LA-ICP-MS U-Pb zircon dating and geochemical characteristics of diabase-dykes from the Qingshuiquan area, Eastern Kunlun Orogenic Belt. *Acta Petrol. Sin.* **2009**, *25*, 1135–1145.
92. Sang, J.Z.; Pei, X.Z.; Li, R.B.; Liu, C.J.; Chen, Y.X.; Li, Z.C.; Chen, G.C.; Yang, S.; Wang, X.B.; Chen, G.; et al. LA-ICP-MS zircon U-Pb dating and geochemical characteristics of gabbro in Qingshuiquan, east section of East Kunlun, and its tectonic significance. *Geol. Bull. China.* **2016**, *35*, 700–710. (In Chinese with English abstract)
93. Song, Z.B.; Zhang, Y.L.; Jia, Q.Z.; Chen, X.Y.; Jiang, L.; Li, D.S.; He, S.Y.; Li, J.C.; Yang, T.; Quan, S.C.; et al. U-Pb age of Yemaquan deep Variscan granodiorite in Qimantage area, eastern Kunlun and its significance. *Geoscience* **2014**, *28*, 1161–1169. (In Chinese with English abstract)
94. Shaanxi Institute of Geological Survey. *Regional Geology of the Ayak Kum Lake Region*; Shaanxi Institute of Geological Survey: Shaanxi, China, 2003; pp. 1–266. (In Chinese)
95. Wang, G.; Sun, F.Y.; Li, B.L.; Li, S.J.; Zhao, J.W.; Cong, Z.C. Petrography, zircon U-Pb geochronology and geochemistry of the mafic-ultramafic intrusion in Xiarihamu Cu-Ni deposit from East Kunlun, with implications for geodynamic setting. *Earth Sci. Front.* **2014**, *88*, 318–319. [CrossRef]
96. Xiong, F.H.; Ma, C.Q.; Jiang, H.A.; Liu, B.; Huang, J. Geochronology and geochemistry of Middle Devonian mafic dykes in the East Kunlun orogenic belt, Northern Tibet Plateau: Implications for the transition from Prototethys to Paleotethys orogeny. *Geochemistry* **2014**, *74*, 225–235. [CrossRef]
97. Xiong, F.H.; Ma, C.Q. Petrological evidence of the deep subduction of the original Tethys oceanic crust in Central East Kunlun. In *Proceedings of the Academic Conference on New Progress in Resource Environment and Geoscience Space Information Technology*; Science Press: Beijing, China, 2016.
98. Zhang, J.X.; Meng, F.C.; Wan, Y.S.; Yang, J.S.; Dong, G.A. Early Paleozoic tectono-thermal event of the Jinshuikou Group on the southern margin of Qaidam: Zircon U-Pb SHRIMP age evidence. *Geol. Bull. China.* **2003**, *22*, 397–405. (In Chinese with English abstract)
99. Zhang, J.Y.; Ma, C.Q.; Xiong, F.H.; Liu, B.; Li, J.W.; Pan, Y.M. Early Paleozoic high-Mg diorite-granodiorite in the eastern Kunlun Orogen, western China: Response to continental collision and slab break-off. *Lithos* **2014**, *210–211*, 129–146. [CrossRef]
100. Zhou, C.J.; Hu, D.G.; Barosh, P.J.; Wu, Z.H.; Zhang, Y.Q.; Geng, J.Z.; Hao, S.; Ni, J.Y.; Zhang, Y.L. Zircon U-Pb dating of the rhyolite-dacite porphyry in the Sandaowan of East Kunlun Mountains and its geological significance. *J. Geomech.* **2010**, *16*, 28–35. (In Chinese with English abstract)
101. Zhu, Y.H.; Lin, Q.X.; Jia, C.X.; Wang, G.C. SHRIMP zircon U-Pb age and significance of Early Paleozoic volcanic rocks in East Kunlun orogenic belt, Qinghai Province, China. *Sci. China Ser. D-Earth Sci.* **2006**, *49*, 88–96. [CrossRef]

Disclaimer/Publisher's Note: The statements, opinions and data contained in all publications are solely those of the individual author(s) and contributor(s) and not of MDPI and/or the editor(s). MDPI and/or the editor(s) disclaim responsibility for any injury to people or property resulting from any ideas, methods, instructions or products referred to in the content.